Modular Hybrid Energy Concept Employing a Novel Control Structure Based on a Simple Analog System

Dorin PETREUS[1], Stefan DARABAN[1], Marcian CIRSTEA[2]

[1]*Technical University of Cluj-Napoca, Memorandumului 28, 400114, Cluj-Napoca, Romania*
[2]*Anglia Ruskin University, East Rd, CB1 1PT, Cambridge, England*
dorin.petreus@ael.utcluj.ro

Abstract—**This paper proposes a novel control topology which enables the setup of a low cost analog system leading to the implementation of a modular energy conversion system. The modular concept is based on hybrid renewable energy (solar and wind) and uses high voltage inverters already available on the market. An important feature of the proposed topology is a permanently active current loop, which assures short circuit protection and simplifies the control loops compensation. The innovative analogue solution of the control structure is based on a dedicated integrated circuit (IC) for power factor correction (PFC) circuits, used in a new configuration, to assure an efficient inverter start-up. The energy conversion system (control structure and maximum power point tracking algorithm) is simulated using a new macromodel-based concept, which reduces the usual computational burden of the simulator and achieves high processing speed. The proposed novel system is presented in this article from concept, through the design and implementation stages, is verified through simulation and is validated by experimental results.**

Index Terms—**DC-DC power converters, photovoltaic systems, analog circuits, wind energy, hybrid power systems.**

I. INTRODUCTION

Hybrid power systems composed of solar and wind energy, which complement each other, offer a feasible alternative to oil produced energy. A hybrid energy system normally consists of two or more renewable energy sources, power converters, a central controller and optional storage elements for ensuring energy security [1].

One method employed to build hybrid energy systems is to use multiport converters. The power flow into the system is adjusted by PWM (Pulse Width Modulation) or phase shift techniques. This method has reduced part count and converter size but it has a centralized and complex control structure [2-3]. Another disadvantage of multiport converters is the fixed hardware structure, which is inflexible to updates; in order to add new functions, the whole multiport converter must be replaced.

A multiport converter is presented in [4].This is either based on a Buck-Boost converter (with wind turbine only or hybrid power source connected) or on a Buck converter (with PV source only connected), depending on the operating state of the system. With such a solution, when implementing the maximum power point tracking (MPPT)

controller, the control of the wind turbine influences the control of the PV source.

Another multiport topology, based on a Sepic converter (tied to the wind turbine) and a Cuk converter (tied to the PV system) is presented in [5].In this topology, the MPPT controllers for the two power sources do not influence one another. However, the problem with Sepic and Cuk converters is their low efficiency.

Instead of connecting multiple power sources to a single converter, another strategy to build hybrid energy systems is to use a separate converter for each power source [6]. The AC and DC buses are also present in this topology. Additional power converters can be added through the DC bus or through the AC bus. For such a hybrid power topology, it is cheaper to replace a single converter when it breaks down.

In [7], the authors eliminated the power converter of the PV system and directly connected the solar panels to the DC-AC converter. The wind turbine is connected to the main inverter through a DC-DC converter. The efficiency of the system is increased and the overall costs are reduced, but the DC bus is eliminated (DC bus voltage is needed for future microgrids).

In [8], the authors proposed a hybrid energy system which connects in series the outputs of the DC-DC converters. The input voltages of the DC-AC inverter can go up to 600V. Stacking high power converters in series is rather dangerous and requires careful design.

A modular power system concept is proposed in this paper, which allows to use high voltage power inverters already available on the market in different applications. Another advantage of the proposed system is the use of the same DC-DC converter (with different MPPT algorithms) for energy harvesting from multiple renewable energy sources.

Firstly, a modular hybrid energy harvesting topology is analyzed in conjunction with an innovative control structure. This is followed by a detailed description of the analog solution of the proposed control structure and its implementation. Simulations and experimental results illustrate the performance of the system based on the novel control structure. The final section provides the conclusions.

II. MODULAR HYBRID ENERGY CONVERSION SYSTEM

There are two methods to implement low cost systems: 1)

use simple power structures with medium/low quality components; 2) use complex but high efficiency power structures, targeting mass production for cost effectiveness. The concept of a modular energy harvesting system is based around using existing systems and adapting them to pre-imposed requirements.

A block schematic representing the concept of a modular system is shown in Fig. 1. Different renewable power sources (wind turbines, solar panels, fuel cells) can make use of the same converter with the same control strategy. The functionality of the whole system can be changed only by modifying the MPPT Card. The MPPT algorithm depends on the energy source [9-11].

The minimum amount of information is transmitted between blocks. The main signals are: power supply voltage (15V), ground (GND), inductor current (the voltage between the two points BS+ and BS- is the voltage drop on the current sensing resistor), DC bus voltage (V_{BUS}), input voltage (V_{IN}), control signal (PWM or V_C) and command from energy management controller (S_x).
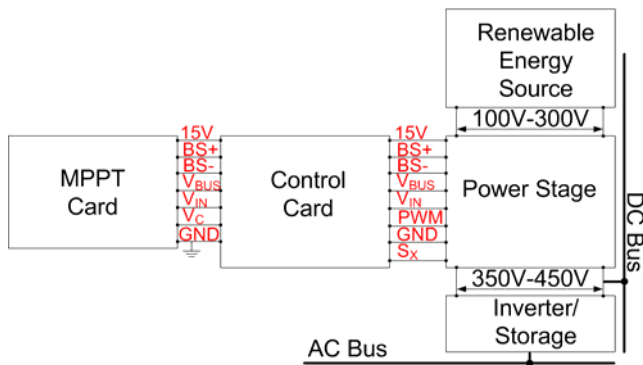

Figure 1. Modular energy conversion system concept.

A modular hybrid energy conversion structure is proposed in Fig. 2. It is shown how the principle from Fig. 1 can be used to implement modular energy harvesting systems. The power converters (composed of a power stage with control card and MPPT card) which harvest energy from the PV source and wind turbine are connected together to a single inverter.

The Coolcept topology (inverter from Fig. 2) is property of Steca Elektronik GmbH [12] and is designed to work as a grid-tied inverter for photovoltaic applications. Because of its high efficiency and already implemented inverter functions, the Coolcept converter will also be used to implement a wind-solar energy conversion system. The Coolcept inverter works as a string inverter for PV panels (scans the entire power-voltage (P-V) characteristic of the photovoltaic panels in case of partial shading). To implement a hybrid energy conversion system, the Coolcept inverter is configured to maintain its input voltage constant.

In Fig. 2, the solar panels are connected to the DC bus through DC-DC converters. These converters can be: Multi String/String technology or power optimizers. The String technology uses bypass diodes to protect the solar panels in case of partial shading. The power optimizers replace the bypass diodes with DC-DC converters in order to increase the energy harvesting capability of the system [13]. Some of the most used power optimizers are: parallel connected [14], series connected [15], Δ converters [16] and micro-inverters
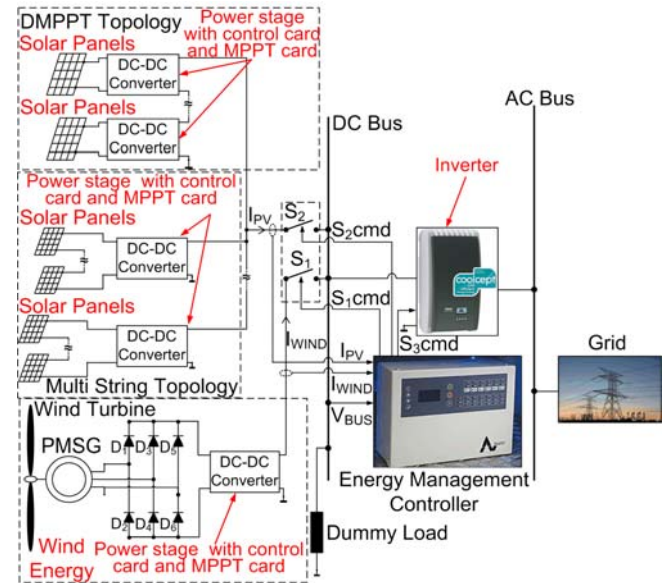
[17].

Figure 2. Proposed modular hybrid energy harvesting system.

The wind energy conversion system (WECS) uses a permanent magnet synchronous generator (PMSG) and an uncontrolled three phase rectifier to obtain a DC voltage at the input of the power converter, which harvests maximum power from the wind turbine when connected to the DC bus.

To implement the modular energy harvesting system, a control structure for the MPPT or DMPPT (Distributed Maximum Power Point Tracking) converters (DC-DC converters from Fig. 2) is needed to control the DC bus voltage when the inverter is not connected to the DC bus. The inverter has to detect at least 350V at its input in order to start. To ensure a proper start-up of the inverter, the energy harvesting converters will control the DC bus first. All three types of energy harvesting converters (WECS, Multi String/String technology, power optimizers) from Fig. 2 implement the same control structure. The main focus of the work presented in this paper is to develop a control structure for interconnecting modular power converters and inverters in order to form a hybrid energy conversion system based on renewable energy sources.

III. PROPOSED CONTROL STRUCTURE

The proposed control topology is illustrated in Fig. 3. This topology will target for a low cost solution implementation. The MPPT card is attached to the control card as illustrated in Fig. 3. The functionality of the whole system can be changed only by modifying the MPPT card. The DC bus voltage loop (Fig. 3) is active when an inverter is not connected to the system. When the energy harvesting converter is tied to the inverter, the sensed output voltage (V_{bus}) will go below the V_{REF} threshold and the output of the PI controller will saturate, thus it will impose a minimum current that has to be extracted from the renewable energy source. If the minimum power level is achieved, the MPPT mode is enabled.

When the inverter gets disconnected from the energy harvesting converter, the DC bus voltage (V_{BUS}) will increase, and the sensed voltage (V_{bus}) will go above the V_{REF} threshold. Now, this voltage (V_{bus}) is regulated by the

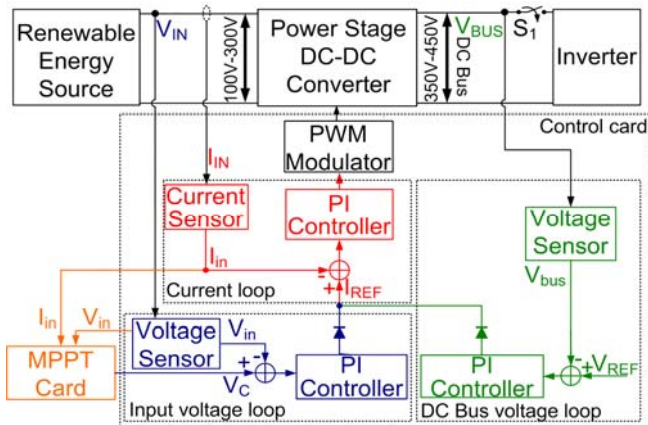DC bus voltage loop (Fig. 3) and the MPPT algorithm is disabled.

Figure 3. Proposed control structure suitable for modular hybrid energy harvesting systems.

The input voltage, V_{IN} (Fig. 3) is controlled when the DC-DC converter is connected to the inverter and the MPPT mode is active. This control structure has to be general and has to apply both to photovoltaic systems (power optimizers or Multi String technology) and to WECS. The only difference between the two systems (solar and wind) is the MPPT algorithm.

With this novel approach to the control topology, the compensation of the system is simplified because both voltage loops (input and output) use the current loop (Fig. 3). When the inverter is connected to the converter, the output voltage loop will reach saturation and will impose a minimum power level that should be extracted from the renewable energy source. If this test is passed, the MPPT algorithm is started; otherwise the system enters the shutdown state. The proposed control topology is used in a modular design and assures an effective start-up for any inverter.

The start-up sequence of the system is illustrated in Fig. 4. The references in the text are made to the schematic shown in Fig. 3. In principle, an automatic analog ORing circuit is implemented to impose the current reference node (I_{REF}) depending on the state of the inverter. The inverter is modeled like a high voltage DC source (because of the internal voltage loop which regulates its input voltage).

When the system starts to operate (t_0), the inverter is disabled and the DC bus voltage loop (Fig. 3) will regulate the DC bus. A small current (I_1) passes through the system because of the connected dummy loads. When switch S_1 connects the inverter to the DC bus (t_1), the inverter starts to regulate this voltage at 360V. At this point, both converters (energy harvesting converter and inverter) are set to regulate the DC bus voltage.

The inverter imposes the voltage on the DC bus (360V) and the energy harvesting converter sets the short circuit current (due to the current loop). At time t_2, the MPPT controller is activated by imposing a voltage reference through V_C. The output of the input voltage loop regulator (Fig. 3) controls the current through I_{REF}. The MPPT algorithm starts at time t_3 and begins to track the optimum operating point.

In order to obtain a low cost system, the proposed control topology is implemented with analog circuitry. This control

structure would be difficult to implement with analog switched mode power supply controllers because they became very specialized and focused on certain applications. Switched mode power supplies represent a domain where integrated circuits (IC) have an important role for improving their performance. By using IC, for implementing the control structure and the gate drivers, the system cost can be reduced.
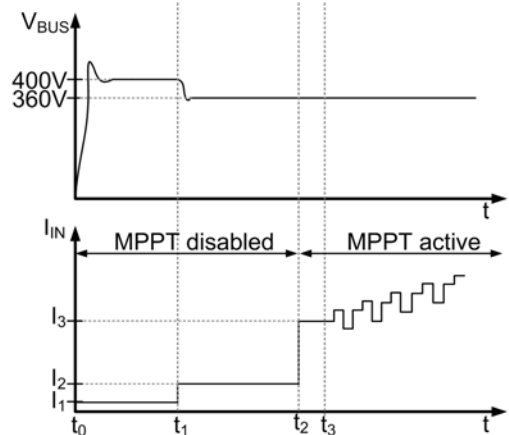

Figure 4. Start-up sequence of the system.

The specialized integrated circuits for PFC usually control the input current and also the DC bus voltage. For this reason, a PFC controller can be adapted to the control structure proposed in Fig. 3. Given that the control structure is aimed for targeting the implementation of systems with power levels up to 2kW or higher, the most relevant PFC regulators that can be used are the ones with average current mode control.

Because a PFC controller is used in a novel configuration (which does not implement the function of power factor correction), not all of its functions will be needed. An example is the feedforward loop implemented on the division pin of the multiplier (which is present in PFC controllers with average current mode control). The role of the feedforward loop implemented in a PFC system is to maintain a constant power when the input line voltage changes. On the other hand, the role of the MPPT system is to perturb the input voltage and find the direction of the maximum power point.

A PFC controller offering increased flexibility in design, at a low cost, is UC3854. The complete schematic of the proposed control structure implemented with UC3854 is presented in Fig. 5. It can be seen that the feedforward loop can be easily disabled by setting the V_{RMS} (8) pin at a fixed voltage. The advantages of using this integrated circuit are: low cost, two error amplifiers with full access to their pins, PWM modulator, peak current protection, driver, under voltage lock out. The proposed control topology implemented with UC3854 can be adapted to be used both in PV system (power optimizer and Multi String technology) and in WECS.

When the DC-DC converter is not connected to the DC bus, the converter controls its output voltage at around 420V. The DC bus is regulated at 360V by the inverter when is active. Two power converters (DC-DC converter and inverter) will try to regulate the same voltage. The first converter which saturates its voltage loop first will impose the current that passes through the system (due to the current

protection) and the other converter will set the operating voltage on the DC bus. In this case, the inverter imposes the voltage on the bus (360V) and the energy harvesting converter will set the short circuit current. Now the inverter is similar to a 360V battery because it accepts all the power from the energy harvesting system and maintains its voltage constant. After the DC bus is regulated by the inverter, the MPPT card switches automatically to MPPT mode.

The proposed structure implementation is presented in the next paragraph.

IV. CIRCUIT DESIGN AND IMPLEMENTATION

The proposed control topology is applied to a wind energy conversion system in order to show that a photovoltaic inverter can be used in WECS.
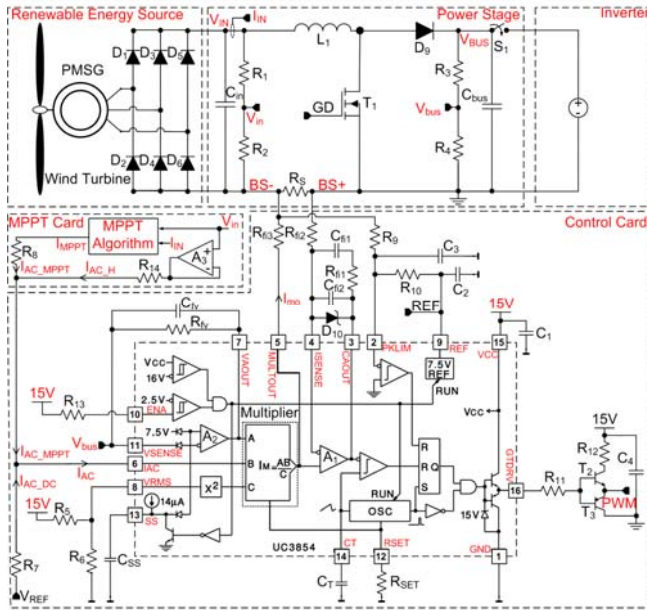

Figure 5. Complete electrical schematic.

The complete system schematic with UC3854 used for energy harvesting is presented in Fig. 5. The system presented in this paper is a proof of concept built for a novel control topology to be used in hybrid energy systems.

A. Power Stage

The maximum power point harvesting circuit is a DC-DC converter and has to be designed accordingly. The full output capability (2kW) can only be extracted for an input voltage in the range of 200V-300V. The converter starts to operate from an input voltage of 100V but the output power capability is limited to 1.25kW. The maximum short circuit current protection occurs at 12.5A. The control structure is tested on a Boost converter, but it can be applied to any DC-DC power converter topology. In principle the input current is controlled (when MPPT mode is active), but at start-up the output voltage is controlled in order to assure the proper start of the inverter. The same principle can also be applied to a step-down convert (Buck) or step-up/step-down converter (Buck-Boost).

For the Boost converter in Fig. 4 a 300μH inductor was used. The input capacitor is 47μF and the output capacitor is 660μF(three in parallel). The parameters for the wind turbine are: L_d and L_q (d and q inductances) are 22mH, the

number of poles is 16 and the moment of inertia is 4kg·m^2. In simulations, the following values were considered for the inverter: the value of each inductor is 300μH, each input capacitor is 660μF and each output capacitor is 47nF.

The significance of some of the parameters used in the design of the energy harvesting system, controlled by a PFC regulator (UC3854), is illustrated in Fig. 6. The MPPT card has two operating modes: when MPPT algorithm is active and when MPPT algorithm is disabled. When the MPPT algorithm is active the average inductor current (I_{L_avg}) is proportional to I_{mo} and to I_{AC} - see also Fig. 4 for I_{mo} and I_{AC} significance. In this state the value of the I_{mo} varies from $I_{mo\_vao\_sat}$ to I_{mo_max} and the value of I_{AC} varies between $I_{AC\_vao\_sat}$ and I_{AC_max}. When the MPPT algorithm is disabled I_{mo} varies between 0 and $I_{mo\_vao\_sat}$ (this value is reached when the DC bus voltage loop is saturated) and I_{AC} varies between 0 and $I_{AC\_vao\_sat}$.
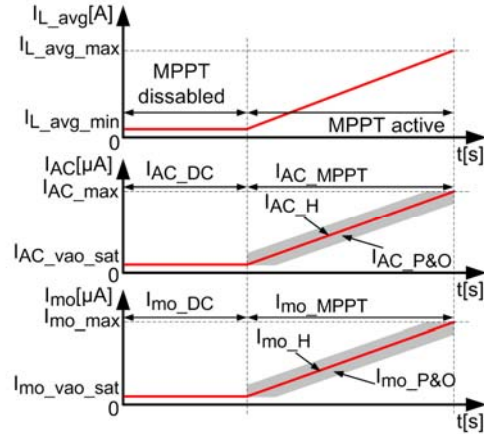

Figure 6. Significance of certain parameters from the design procedure.

B. Inverter

The simplified schematic of the Coolcept inverter is presented in Fig. 7. There are two symmetrical Buck converters (T_1, C_1, D_1, L_1, C_3 and C_2, T_2, D_2, L_2, C_4) which are placed one on top of the other. By dividing the input and output voltage in half for the two converters, semiconductors with lower voltage rating can be used, thus obtaining higher performance. A rectified sinusoidal voltage is present at the output of the Buck converter. This voltage is then unfolded by the H-bridge (S_1, S_2, S_3 and S_4) and a sinusoidal voltage is obtained at the output.

To implement a hybrid energy conversion system, the Coolcept inverter is configured to maintain its input voltage constant. This is why the inverter is represented in all schematics by a DC voltage source.
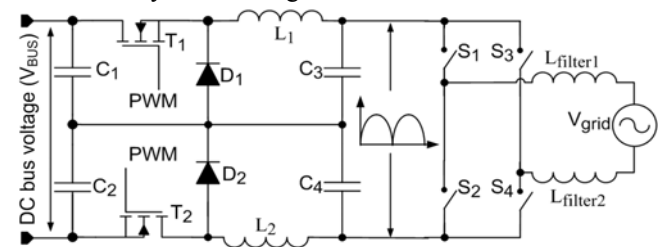

Figure 7. Coolcept inverter simplified schematic.

C. Control Card

The multiplier is used in a novel configuration, thus the sizing is very important. The voltage at pin named I_{AC} is kept constant at 6V and the current through this pin is

considered the input 'B' of the multiplier. The I_{AC} current is composed from two components (Fig. 5): I_{AC_DC} which is the DC offset value of the current through I_{AC}; I_{AC_MPPT} is the current from the MPPT card. The multiplier output current has the same two components: I_{mo_DC} and I_{mo_MPPT}. The relation between the multiplier output current (I_{mo}) and the current through I_{AC} is described by:

$$I_{mo} = \frac{I_{AC} \cdot (VA_{Out} - 1)}{V_{rms}^2} \quad (1)$$

where VA_{Out} is the output of the DC bus error amplifier A_2 (Fig. 5) and V_{rms} is the voltage at the V_{RMS} pin, which is also input 'C' of the multiplier.

The maximum recommended current value through I_{AC} is 0.6mA. It is also recommended for I_{AC} to be as high as possible, because at high current the best linearity is achieved. Because the calculated component values are not always standard values and because of their tolerances, the system must be able to work in a linear zone and not saturate. For calculations purpose: 0.5mA is chosen as value for I_{AC_max} and 0.2mA is chosen for I_{mo_max}.

The multiplier's output is inhibited if the output voltage of the error amplifier is bellow 1V. When the inverter is connected to the Boost converter, the output of the voltage error voltage amplifier saturates at 5.8V. The voltage at the V_{RMS} pin is calculated with:

$$V_{RMS} = \sqrt{\frac{I_{AC\_max} \cdot (5.8 - 1)}{I_{mo\_max}}} \quad (2)$$

The R_{SET} resistor sets the maximum multiplier current:

$$R_{SET} = \frac{3.75V}{I_{mo\_max}} \quad (3)$$

The current error amplifier build around amplifier A_1 (Fig. 5) is configured as a proportional-integrator. The average value of the negative input of this error amplifier is zero because this voltage is pulled to ground by R_{fi2}. Due to the negative feedback, the positive input will be made equal to the negative input. The output of the multiplier is a current source, thus the positive input of the current error amplifier (A_1 from Fig. 5) can be expressed by:

$$V_+ = R_S \cdot I_{IN} + R_{fi3} \cdot I_{mo} \quad (4)$$

where R_S is the current sense resistor and I_{IN} is the average inductor current (for a Boost converter is also the input current). Due to the negative feedback the two inputs of the error amplifier are equal and due to the proportional integrative structure are equal to zero.

The value of resistor R_{fi3} is calculated by:

$$R_{fi3} = \frac{R_S \cdot I_{IN}}{I_{mo}} = \frac{R_S \cdot I_{L\_avg\_max}}{I_{mo\_max}} \quad (5)$$

By replacing (5) in (1), the average value of the inductor current is:

$$I_{IN} = \frac{R_{fi3} \cdot I_{AC} \cdot (VA_{Out} - 1)}{R_S \cdot V_{rms}^2} \quad (6)$$

The input current as a function of the I_{AC} current is:

$$I_{IN} = \frac{R_{fi3} \cdot (VA_{Out} - 1)(I_{AC\_DC} + I_{AC\_MPPT})}{R_S \cdot V_{rms}^2} \quad (7)$$

$$I_{IN} = \frac{R_{fi3} \cdot (VA_{Out} - 1)}{R_S \cdot V_{rms}^2} \cdot \left(\frac{7.5V - 6V}{R_7} + I_{AC\_MPPT} \right) \quad (8)$$

where 7.5V is the voltage reference of UC3854 (V_{REF}).

When the DC-DC converter is connected to the inverter and the MPPT is disabled, the power of the converter is limited by design because of resistor R_7. The average current through the inductor must be limited to $I_{L\_avg\_min}$. By using Fig. 6 and also keeping in mind that R_7 is connected between the I_{AC} pin (internally maintained at 6V by UC3854) and the voltage reference (7.5V) of the UC3854 controller, R_7 is calculated with:

$$R_7 = \frac{(7.5V - 6V)}{I_{AC\_vao\_sat}} \quad (9)$$

D. MPPT Card

The functionality of the system can be changed by implementing a different MPPT algorithm in the MPPT card. Depending on the energy source used (wind energy, photovoltaic energy, fuel cells), an adequate tracking algorithm is implemented with suitable perturbation step and decision time.

A MPPT algorithm for WECS is proposed, which uses both software and hardware (Fig. 5). A Perturb and Observe (P&O) algorithm is implemented in a low cost microcontroller. The current from this component is marked as $I_{AC\_P\&O}$ and passes through R_8.

The Current-Voltage (I-V) characteristic of a wind turbine, measured after the three phase rectifier and capacitive filter, are represented in Fig. 8. After a certain power level, the maximum power point varies almost linearly from a characteristic to the other. The MPP trajectory is used to calculate the second component of I_{AC_MPPT} from Fig. 5 (I_{AC_H}). The slope of the locus of the maximum power point on the I-V characteristic is used to calculate the resistance needed to implement the hardware component (I_{AC_H}). The points marked on the two characteristics (in Fig. 8) represent the maximum power points. If the maximum power points are not on the MPP trajectory, these points are searched with high accuracy by the P&O algorithm. The searching area of the P&O is marked in grey in Fig. 6 and in Fig. 8a).
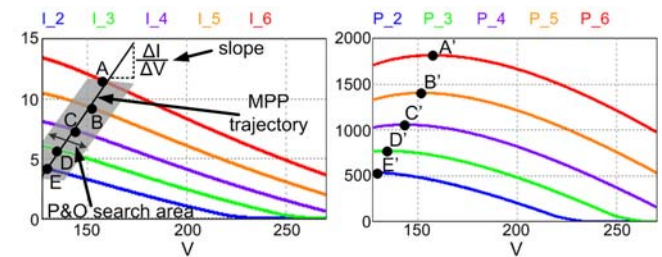

Figure 8. Wind turbine characteristics. (a) I-V. (b) P-V.

As seen in Fig. 5 and Fig. 6, the current through R_7 is an offset and the currents through R_8 and R_{14} form the I_{AC_MPPT} current. The I_{AC_MPPT} is calculated with:

$$I_{AC\_MPPT} = I_{AC\_H} + I_{AC\_P\&O} = \frac{G_{div} \cdot V_{IN} - 6V}{R_{14}} + \frac{I_{MPPT\_max} - 6V}{R_8} \quad (10)$$

where V_{IN} is the input voltage with no voltage divider gain, G_{div} is the input voltage divider gain composed of R_1 and R_2 (Fig. 5). The output of the MPPT card is a voltage that sets the current reference for the current loop when the MPPT algorithm is active. Because the MPPT card sets a current reference the name was set I_{MPPT} (measured in Volts). The

maximum value of I_{MPPT} is proportional to the maximum current through R_8:

$$R_8 = \frac{I_{MPPT\_max} - 6V}{I_{AC\_P\&O}} \qquad (11)$$

where $I_{AC\_P\&O}$ (represents the grey area from Fig. 6 and Fig. 8a) is chosen around $0.1 \cdot I_{AC\_max}$. The proposed MPPT algorithm includes both software and hardware solutions. The MPP locus from Fig.8a is an approximation of the real MPP locus that can be found in practice. In order to take into account the small differences that can occur in a real wind turbine the P&O algorithm will adjust the deviation only by a small amount. An error of 10% was considered.

It is assumed that I_{MPPT} command does not have a large variation from one operating point to the other. Using (8) and (10) to calculate the current and the voltage of the operating points 'A' and 'E' from Fig. 8a), and then subtracting them, will lead to:

$$\Delta I = \frac{R_{fi3} \cdot (VA_{Out} - 1)}{R_S \cdot V_{rms}^2} \cdot \frac{G_{div} \cdot \Delta V}{R_{14}} \qquad (12)$$

where ΔI is the variation of the input current and ΔV is the variation of the input voltage (Fig. 8a). The voltage divider gain for the input voltage is calculated such that the voltage in the 'E' operating point, after it gets divided, will be small enough not to produce a current for I_{AC}:

$$V_E \cdot G_{div} = V_E \cdot \frac{R_2}{R_1 + R_2} = 6V \qquad (13)$$

where V_E is the voltage in the 'E' operating point of Fig. 8a). The compensation of the control loop has been calculated in [18].

V. SIMULATION RESULTS

In order to speed up simulation times and simulate a hybrid energy conversion system that contains multiple power converters [19], a macromodel is proposed for the systems containing the control topology proposed in Fig. 5. Due to the current loop being always active, whether the input voltage or DC bus voltage is controlled or not, the DC-DC converter can be replaced with a voltage controlled current source. The schematic of the proposed macromodel is presented in Fig. 9.
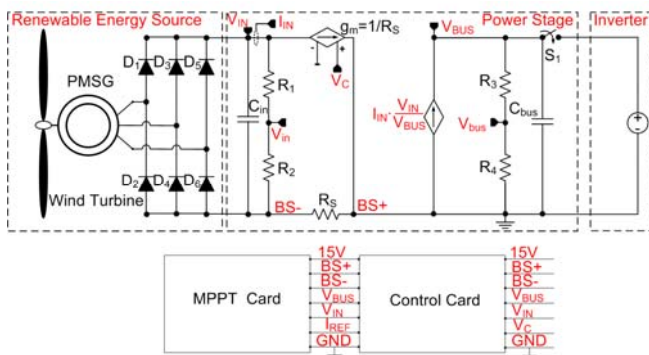

Figure 9. Proposed macromodel.

The current source with the gain $1/R_S$ receives the command from UC3854. The same model for UC3854 is used, but the command voltage (V_C) is no longer the PWM signal but the voltage on the R_{fi3} resistance (Fig. 9), calculated using equation (5). The voltage controlled current

source (with gain $I_{IN} \cdot V_{IN}/V_{BUS}$) assures that the input power of the converter is equal to its output power.
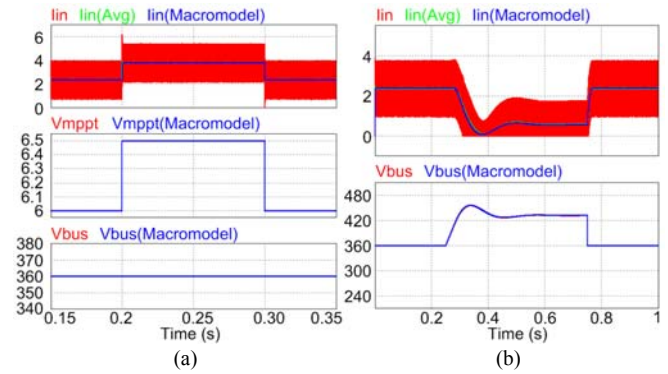

Figure 10. Simulation with macromodel and switching circuit. (a) MPPT mode active. (b) Connection and disconnection from inverter.

To validate the macromodel, the results of testing the actual switching converter are compared to the results of the macromodel. For the simulations in Fig. 10a), the switching converter and the macromodel are in MPPT mode. The MPPT algorithm changes the current reference. The waveform Iin(Avg) averages the switching inductor current waveform (red) and it is identical to the current waveform of the macromodel (blue). For the wavefoms illustrated in Fig. 10b), the converter is connected/disconnected to/from the inverter. It can be seen that the transient responses of the macromodel and those of the real circuit are identical. The macromodel averages the waveforms of the power converter and the simulation time can be reduced up to 40 times.

In this way, multiple converters can be easily added to the model/system and energy management algorithms can be tested and compared much faster with macromodels, instead of using real converters. The response of the system with the proposed MPPT algorithm to a wind speed change is presented in Fig. 11. It can be seen that the maximum power point is tracked by the proposed algorithm. The response of the MPPT algorithm and of the control structure is presented in Fig. 11b). With the hardware component (amplifier A_3 and R_{14} from Fig. 5) and the simple MPPT algorithm, the system finds the new maximum power point.

In order to evaluate the performance of the proposed MPPT algorithm, a simulation is made with a wind pattern [20]. The results are illustrated in Fig. 12. The first waveform shows the extracted power (Pin) and the total power (Optimum) present at the input of the system. The other two waveforms show how the voltage of the optimum operating point changes when the wind speed changes. Good tracking performance is obtained.
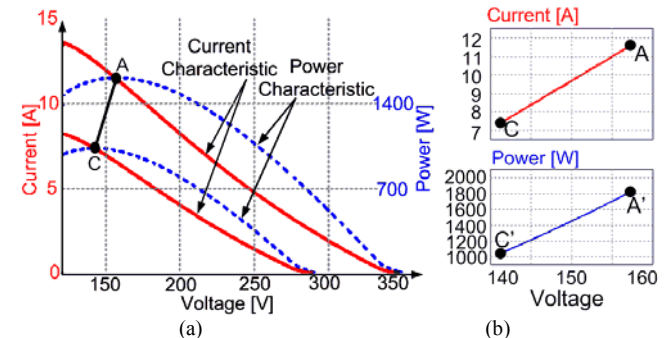

Figure 11. System response to a wind speed change. (a) With proposed MPPT algorithm. (b) Simulation.
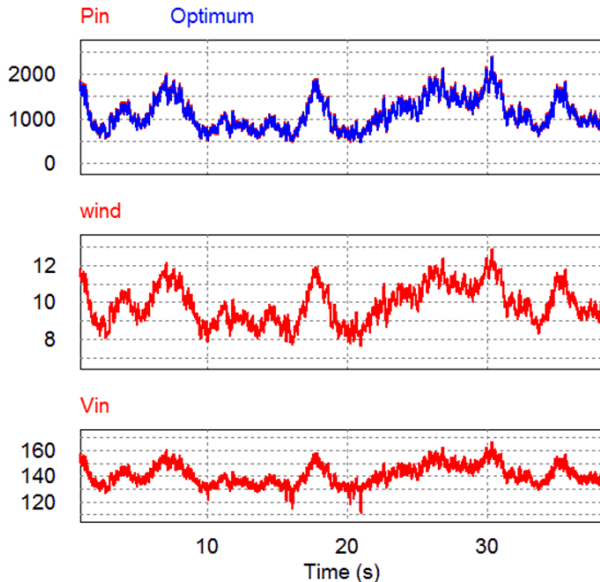
Figure 12. MPPT algorithm simulation with wind speed model.

VI. PERFORMANCE TESTING

In order to test the proposed control structure (as a proof of concept) for implementing modular hybrid energy harvesting systems, an experimental setup is developed. This control topology can be also applied to power optimizers and Multi String/String technology for photovoltaic systems and also to WECS. The simulation (Fig. 13a) and experimental (Fig. 13b) results of the start-up sequence are presented in Fig. 13. These results are closely related to the theoretical waveforms presented in Fig. 4.

At time t_0, the DC bus voltage is controlled by the energy harvesting converter. After the inverter is connected to the DC bus (t_1), the DC bus voltage is maintained constant by the inverter. The energy harvesting converter initializes the MPPT mode (t_2) and then starts the tracking of the MPP (t_3).
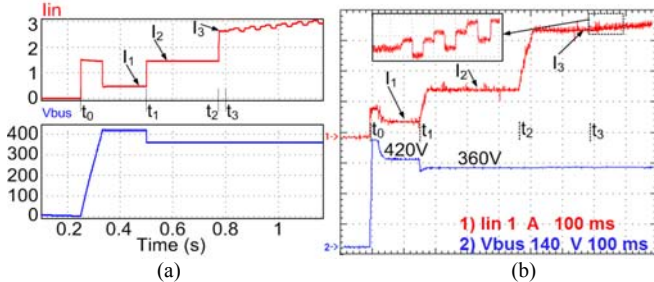

Figure 13. Start-up sequence of the system. (a) Simulation results. (b)

When the DC-DC converter is not connected to the inverter, the extracted current is imposed by the dummy load and the DC bus voltage is maintained at 420V or higher. When the inverter is active, the DC bus voltage is imposed at 360V and the MPPT algorithm is activated, thus increasing the input current. The simulation (Fig. 14a) and experimental (Fig. 14b) results for the connection/ disconnection of the DC-DC converter to/from the inverter are presented in Fig. 14.

When the DC-DC converter is tied to the inverter, the MPPT algorithm is active and the maximum power is harvested from the renewable power source. In this state, the DC bus voltage is regulated by the inverter. For any perturbations in the system, the inverter will try to maintain a constant DC voltage. The simulation results, which show how the inverter regulates the DC bus when the MPPT algorithm perturbs the current reference, are illustrated in

Fig. 15a). The experimental results are presented in Fig. 15b).
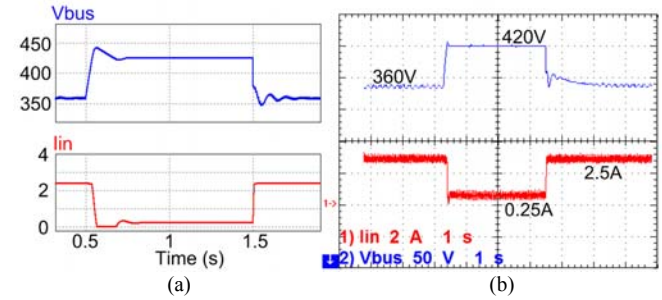

Figure 14. Connection and disconnection from inverter. (a) Simulation results. (b) Experimental results.

If the perturbation step size is high enough in the MPPT mode, the power change can be seen even at the output. The perturbation step of the MPPT algorithm is proportional to the change of the input current and the grid injected current. The simulation and experimental results are presented in Fig. 16a) and Fig. 16b) respectively.

The grid voltage and the grid injected current are presented in Fig. 17. For both simulations (Fig. 17a) and experimental (Fig. 17b) results, the power factor is close to unity.
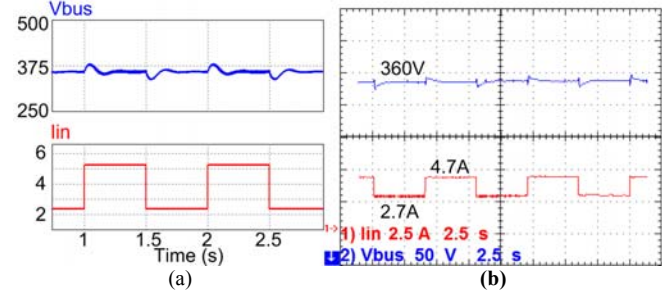

Figure 15. DC bus regulation when the MPPT algorithm is active. (a) Simulation results. (b) Experimental results.

The experimental setup is illustrated in Fig. 18. Every component of the system is labelled with a number. It can be seen that the DC-DC converter is tested with a DC voltage source. The AC voltage from an outlet is passed through an autotransformer (which is a high inductance) and then rectified and filtered. The input voltage is in the range of the wind turbine (100V-300V). When a wind turbine is connected, there is no galvanic connection between the power source and the inverter. For the DC voltage source, an outlet with galvanic isolation has been used because the inverter is transformerless. The measuring equipment also has galvanic isolation.
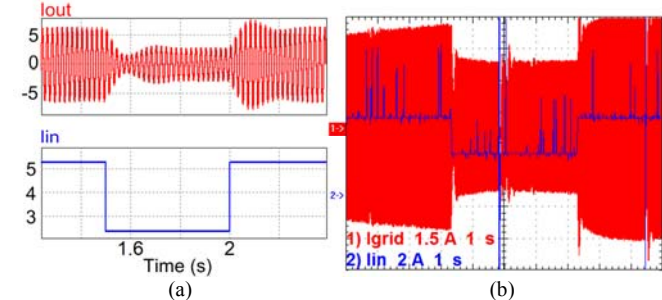

Figure 16. Variation of the grid current with the steps of the MPPT algorithm.(a) Simulation results.(b) Experimental results.

The inverter tied to the grid is transformerless. In a real energy harvesting application the solar panels/wind turbines are isolated from the grid so no additional galvanic isolation is needed. The experimental setup in the laboratory uses as input power source a high voltage source (100V – 300V)

supplied also from the grid that contains a rectifier with a capacitive filter.
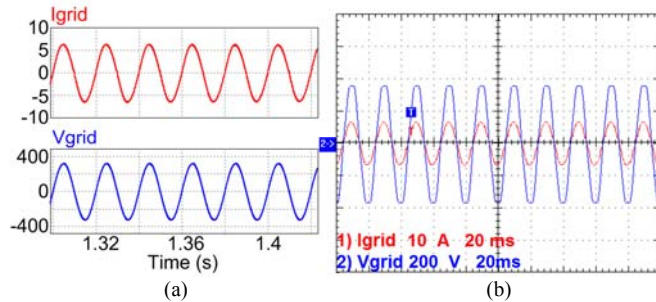

Figure 17. Grid voltage and current injected into the grid.(a) Simulation results.(b) Experimental results.
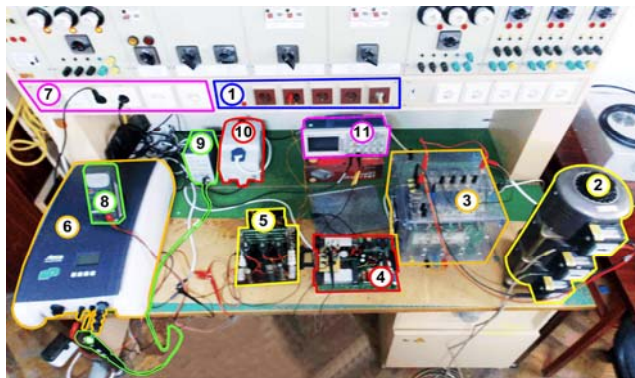

Figure 18. Experimental setup.

The following equipment is used to test the proposed system: 1. Outlets with galvanic isolation; 2. Autotransformer; 3. Rectifier with capacitive filter; 4. Proposed DC-DC converter; 5. Dummy load; 6. StecaGrid3600 inverter; 7. AC outlet; 8. Multimeter; 9. Current probe; 10. Isolation transformer; 11. Oscilloscope.

VII. CONCLUSION

A modular hybrid energy conversion concept is proposed, which is based on components commercially available and reuse them with different purposes or in different applications. An inverter built only for solar applications was used to build a hybrid energy conversion system. This was possible, only by using the proposed novel control topology to implement a modular hybrid energy system.

One of the most important features of the proposed topology is the current loop, which is always active. It assures short circuit protection and simplifies the compensation of the control loops. This control structure assures a proper start-up of the inverter. A solution that uses a specialized integrated circuit for PFC in a novel configuration in order to implement the desired control structure is proposed. A PFC regulator was chosen because its internal structure eases the implementation of the proposed control structure. Only a few passive components have to be added to the UC3854 to build the proposed control structure. The MPPT card attached to the control card (with UC3854) can change the functionality of the whole system: different MPPT algorithms for energy harvesting, PFC controller.

A macromodel is used instead of the switching converter in order to reduce the simulation times. With the help of the macromodel all the converters can be added in the schematic and simulate the hybrid energy conversion system much faster. The created macromodel corresponds to the model of the proposed control structure.

REFERENCES

[1] P. Shamsi and B. Fahimi, "Stability assessment of a DC distribution network in a hybrid micro-grid application," IEEE Trans. on Smart Grid, vol. 5(5), pp. 2527-2534, 2014. doi:10.1109/TSG.2014.2302804
[2] W. Li, J. Xiao, Y. Zhao, and X. He, "PWM plus phase angle shift (PPAS) control scheme for combined multiport DC/DC converters," IEEE Trans. Power Electron, vol. 27, no. 3, March 2012. doi:10.1109/TPEL.2011.2163826
[3] C. Zhao , S.D. Round, and J.W. Kolar, "An isolated three-port bidirectional DC-DC converter with decoupled power flow management," IEEE Trans. Power Electron., vol 23, no. 5, pp. 2443-2453, 2008. doi:10.1109/TPEL.2008.2002056
[4] Y.M. Chen, Y.C. Liu, S.C. Hung and C.S. Cheng, "Multi-input inverter for grid-connected hybrid PV/wind power system," IEEE Trans. Power Electron. vol.22, no. 3. pp. 1070-1077, May 2007. doi:10.1109/TPEL.2007.897117
[5] J. Hui, A. Bakhshai, and P.K. Jain, "A hybrid wind-solar energy system: a new rectifier stage topology," APEC, 2010, pp. 155-161.
[6] S. Daraban, D. Petreus, and C. Orian, "Control topology for high efficiency small scale wind energy conversion systems," in OPTIM, May 2014, pp. 1070-1077. doi:10.1109/OPTIM.2014.6850945
[7] S.G. Malla, and C.N. Bhende, "Voltage control of stand-alone wind and solar energy system," Electrical Power and Energy Systems vol. 56, pp. 361-373, 2014. doi:10.1016/j.ijepes.2013.11.030
[8] Z. Wang, Z. Zou, and Y. Zheng, "Design and control of a photovoltaic energy and SMES hybrid system with current source grid inverter," IEEE Trans. Appl. Supercond. vol. 23, no. 3, pp. 1051-1055, 2013. doi:10.1109/TASC.2013.2250172
[9] S. Daraban, D. Petreus, and C. Morel, "A novel MPPT (maximum power point tracking) algorithm based on a modified genetic algorithm specialized on tracking the global maximum power point in photovoltaic systems affected by partial shading," Energy,vol.74, pp. 374-388, 2014. doi:10.1016/j.energy.2014.07.001
[10] B. Somaiah and V. Agarwal, "Recursive Estimation-Based Maximum Power Extraction Technique for a Fuel Cell Power Source Used in Vehicular Applications," IEEE Trans. on Power Electron., vol 28, no. 10, pp. 4636-4643, Oct.2013. doi:10.1109/TPEL.2012.2236688
[11] J. Chen, J. Chen and C. Gong, "Constant-Bandwidth Maximum Power Point Tracking Strategy for Variable-Speed Wind Turbines and Its Design Details," IEEE Trans. Power Electron., vol. 60, no. 11, pp. 5050- 5058, Nov. 2013. doi:10.1109/TIE.2012.2225401
[12] Steca Elektronik GmbH – "Steca PV grid Connected".
[13] S.M. MacAlpine, R.W. Erickson, and M.J. Brandemuehl, "Characterization of power optimizer potential to increase energy capture in photovoltaic system operating under nonuniform conditions,"IEEE Trans. Power Electrons.,vol.28, no.6, pp.2936-2945, June 2013. doi:10.1109/TPEL.2012.2226476
[14] K.C. Tseng, C.C. Huang, and W.Y. Shih, "A high step-up converter with a voltage multiplier module for a photovoltaic system," IEEE Trans. Power Electron., vol. 28, no. 6, pp. 3047-3057, June 2013. doi:10.1109/TPEL.2012.2217157
[15] M. Balato, and M. Vitelli, "Optimization of distributed maximum power point tracking PV application: the scan of the power vs. voltage input characteristic of the inverter," Electrical Power and Energy Systems, vol. 60, pp. 334-346, April 2014. doi:10.1016/j.ijepes.2014.03.058
[16] P.S. Shenoy, K.A. Kim, B.B. Johnson, and P.T. Krein, "Differential power processing for increased energy production and reliability of photovoltaic system," IEEE Trans. Power Electrons., vol. 28, no.6, pp. 2968-2979, June 2013. doi:10.1109/TPEL.2012.2211082
[17] H. Hu, S. Harb, N.H. Kutkut, Z.J. Shen, and I. Batarseh, "A single-stage microinverter without using electrolytic capacitors," IEEE Trans. Power Electron., vol. 28, no. 6, pp. 2677-2687, June 2013. doi:10.1109/TPEL.2012.2224886
[18] D. Petreus, T. Patarau, S. Daraban, C. Morel, and B. Morley, "A novel maximum power point tracker based on analog and digital control loops," Solar Energy, vol. 85, no. 3, pp. 588-600, March 2011. doi:10.1016/j.solener.2011.01.005
[19] K. Anderson, J. Du, A. Narayan and A. El Gamal, "GridSpice: A distributed simulation platform for the Smart Grid," Trans. Ind. Informat., vol. 10, no. 4, pp. 2354-2363, June 2014. doi:10.1109/TII.2014.2332115
[20] P. Gavriluta, S. Spataru, I. Mosincat, C. Citro, I. Candela, P. Rodriguez, "Complete methodology on generating realistic wind speed profiles based on measurements," Renewable Energy & Power Quality Journal, vol. 10, pp. 828-833, 2012.